Advances in Basic and Applied Sciences 2 (2024) 59-66

Advances in Basic and Applied Sciences

journal homepage: https://abas.journals.ekb.eg/

Fabrication of low-cost Quantum Dot Sensitized Solar cells (QDSSCs)

Amira. Sh. Ebaid[1*], Ahmed A. El-Hamalawy[2], Meawad M. ElKholy[2,3], Shaker Ebrahim[4], Jehan El Nady[5]

[1]*Higher Institute of Engineering and Technology, Menoufia, Egypt.*
[2]*Physics Department, Faculty of Science, Menoufia University, Shebin El-Koom, Menoufia, 32511, Egypt.*
[3]*Physics Department, Faculty of Science, New Mansoura University, Dakahlia, Egypt.*
[4]*Department of Materials Science, Institute of Graduate Studies and Research, Alexandria University, Alexandria, Egypt.*
[5]*Electronic Materials Department Advanced Technology and New Materials Research Institute, City of Scientific Research and Technological Applications (SRTA-City), New Borg El-Arab City, P.O. Box 21934, Alexandria, Egypt.*

ARTICLE INFO

Article history:
Received 22 October 2023
Received in revised form 30 November 2023
Accepted 30 November 2023
Available online 31 January 2024

doi: 10.21608/ABAS.2023.243952.1032

Keywords: Core; Core/shell; CuInS/ZnS; Solar Cells

ABSTRACT

In this study, low cost and safe quantum dots sensitized solar cells QDSSCs were formulated. Two structures of alloy quantum dots (QDs) (i.e., core and core/shell) were investigated for titanium dioxide (TiO_2) based QDSSCs. The synthesizing of CuInS (CIS) core QDs and CuInS/ZnS (CIS/ZnS) core/shell QDs were formulated via inorganic method. Using the core/shell structure CIS/ZnS for sensitizing TiO_2 photoanode has a significant impact on the QDSSCs overall parameters such as open circuit voltage, short circuit current density and cell efficiency. This is because electrons injecting from the conduction band of the CIS/ZnS to that of TiO_2 is easier than that from CIS to TiO_2 nanoparticles and charge recombination reduction occurs at the interface between photoanode and electrolyte. The J-V curves suggest that the TiO_2/ CIS/ZnS QDSSC exhibits the best photoelectric performance with V_{oc} = 0.17 V, J_{sc}= 5.89 mAcm^{-2} and η = 0.23% which are significantly higher than those of CIS/ TiO_2 QDSSC.

.

1. Introduction

In recent years, alternative sources of energy gain significant

* **Corresponding author E-mail:** amira.ebaid@bie.edu.eg, am_shawky@yahoo.com

interest owing to the global warming. Solar cells are the most favored option among the alternative energy sources because of its simple handling devices, low cost, and lack of carbon dioxide emission [1]. Quantum dot-sensitized solar cell (QDSSCs), a third generation photovoltaic technology, seem to have good potentiality for future implications [2–9] due to their various intrinsic advantages, including elevated absorption coefficient [10], tunable band gap [11–13], easy and cheap production [14] but, the QDSSC performance is depending mainly on the choice of sensitizers and electrolyte [15], Consequently, improving QDSSC performance attracted the attention of several researchers. A standard QDSSC resembles dye sensitized solar cells that comprise a photoanode sensitized with semiconductor, a counter electrode and an electrolyte inserted between both electrodes. Iodide/triiodide (I^-/I_3^-) electrolyte redox couple has extensive applications within dye-sensitized solar cells [16]. But, this couple (I^-/I_3^-) seems to be not appropriate for QDSSCs, where it induces quantum dots (QDs) corrosion and photodegradation [17,18]. Therefore, polysulfide redox couples (S^{2-}/S_n^{2-}) are commonly utilized for QDSSCs to attain satisfactory photon-to-current conversion efficiency with no QDs degradation [19–21]. The photoanode accounts for a conducting glass characterized by having a mesoporous TiO_2 layer connected to QDs sensitizer. There are several semiconductor materials utilized in QDs as sensitizers including, CdS [22], CdSe [23], Ag_2S [24], $CuInS_2$ [25], and PbS [26]. Copper indium sulfide (CIS) QDs are triple compound semiconductors characterized by being free toxic of metal ions [27,28]. QDs exhibit photoluminescence (PL) emission that spans from the visible into the near-infrared range, providing a broad spectrum of light emission [29]. It could tolerate band gap via governing the doping process and the copper-to-indium ratio [30]. Wide band gap ZnS may be utilized as shells to coat and provide protection to CIS QDs because of the coincidence between the lattice parameters and lowered toxicity [31]. The QDSSC has a straightforward mechanism. Upon illumination, the QD undergoes the electron-hole pairs creation. The excited electrons underwent shift into the QD conduction band but the hole still presents within the valence band. Afterwards, the electrons are released out the QD conduction band into the TiO_2 conduction band. The electrons infiltrate additionally within the TiO_2 network till reaching to the conductive glass and move further throughout the external load and close the circuit at the end via returning at the counter electrode [32]. Unfortunately, charge recombining at the QDs electrolyte interface and recombining in the photoanode/electrolyte interface prevent the electrons from taking its normal bath way and subsequently the QDSSC efficiency decreases. As charge recombining at the interface of the electrolyte and photoanode considers the key aspect influencing the QDSSC photovoltaic performance negatively, it is critical to eradicate this type of recombination. The approaches adopted for this purpose include passivating the surface of the photoanode with ZnS [33], utilizing various TiO_2 nanoparticles sizes [34], deposition of a scattering layer [35], and treating via titanium tetra chloride [36]. In this work, ZnS shells were introduced to cover CIS QDs forming core/shell structure. Both CIS core and CIS/ZnS core/shell structure were studied and a positive effect in performance was observed by using the core /shell structure than using only core structure. Thorough investigations on the optical, structured characteristics and morphology of the fabricated photoanodes have been reported.

2. Materials and Methods

2.1 Materials

Across organic company provided Indium chloride tetrahydrate (97.90%), Copper chloride (99%), and 1-mercapto acetic acid (MAA) (99%) for the experiment. Sodium sulfide was obtained from a chem-lab. Zinc acetate dehydrate (98.5%) was obtained from oxford company. Titanium (IV) oxide, anatase nano powder having particles < 25 nm, 99.7% and Acetic acid were supplied from Sigma Aldrich. Ethyl cellulose, ethoxyl content 48% 10 cpc. Alpha-terpineol 97%, and Sulfer, 99.5+%, refined were obtained from New Jersey, USA. Potassium chlorate, sodium hydroxide, and copper II acetate were supplied from El-Nasr Company. Alalmia company supplied isopropanol with a purity of 99.5%, while the international company for sup. & med. Industries provided ethanol with a purity of 99.9%. The transparent glass coated with fluorine-doped SnO_2 (FTO), measuring 2.2 mm in thickness and having a sheet resistance of 14 Ω /sq, was purchased from SOLARNIX in Switzerland.

2.2 Preparation of CuInS and CuInS/ZnS QDs

CuInS QD_s formulation involved a straightforward aqueous solution procedure. In brief, 0.6 ml Cl_34H_2O stock solution (0.1M) was mixed within deionized water (10 ml). In addition, 1 ml MAA (45mM) were admixed with $CuCl_2$ (0.1ml, 0.1M) 0.5 ml MAA (45mM) within deionized water (10 ml). To eradicate the solution turbidity, 9.0 PH was maintained by 1M NaOH. The $CuCl_2$ solution was inserted into $InCl_3$ solution and stirred for 3 min. afterwards; the Na_2S solution (0.5 ml, 0.04 mmol) underwent admixing with the abovementioned reaction solution within room temperature and stirred vigorously for 5 min. Then, the CIS core structure is being ready to use. In order to attain CIS/ZnS core/shell structure QDs, the reaction mixture underwent heating (90˚C) for 30 minutes and 1ml of 0.04 M zinc acetate dehydrate was then supplied wisely and stirred continuously for 5 min. The reaction mixture color had altered gradually from colorless through yellowish and finally it became brown.

2.3 Preparation of TiO_2 /CuInS and TiO_2 /CuInS/ZnS sensitized photoanodes

The TiO_2 photoanodes were synthesized on ultrasonically-cleaned FTO glass slides. The cleaning process of the FTO

substrates take placed through four steps. Firstly, sonication within a soap solution; secondly, sonicating within a deionized water, thirdly, sonicating within isopropanol and finally, by sonicating within ethanol for 30 min in every time. Subsequently, substrates undergo heat treatment (150 °C) for 30 minutes and set aside until cooling occurred. To formulate TiO_2 paste, 0.5 gm of well ground TiO_2 powder underwent dispersing with ethyl cellulose (0.25 gm) in 1.5 mL Alpha-terpineol and 0.1 mL acetic acid and some ethanol drops. The resulting paste was then implemented on the FTO and sintered for 30 min at 450 °C. After cooling down to room temperature, some substrates underwent soaking within the prepared CuInS QDs solutions and the other were immersed in the prepared CuInS/ZnS QDs solutions for 24 hours. After that the photoanodes were rinsed by deionized water and left for drying within room temperature.

2.3 *Electrolyte and Counter electrode*

A polysulfide electrolyte was formulated from 0.05 M KCl, 0.1 M S, and 0.5 M Na_2S aqueous solutions. Cu_2S counter electrode was formulated via spin coating the FTO substrates with aqueous solutions of 200 µL copper acetate (0.5M) and 100 µL of Na_2S (0.5M) at a speed of 1000 rpm for 30 sec alternatively, within room temperature, and then annealed thermally at 300 °C for 5 min.

2.4 Characterization

The UV-Vis spectrophotometer (Evaluation 600 double beam scanning spectrophotometer, Thermo scientific, USA) was employed to acquire the spectra of the optical absorption. The scanning of the light source wavelength ranged from 400 to 1000 nm. A 543 nm excitation wavelength was employed to stimulate the prepared QDs. The x-ray diffraction (XRD) was employed for evaluating the synthesized QDs in terms of crystallinity and crystallite size. High resolution Scanning Electron Microscopy (SEM) technique was adopted for studying the structural morphology and surface of the prepared samples. The FEI Quanta FEG 250 instrument was utilized to perform the analysis experiments. The photovoltaic cells' current density-voltage curves have been evaluated using Autolab potentiostat (origaflex, OGFOSA, France) controlled by Origamaster 5software. A bias voltage is swept typically from -0.5 V to 1.0 V. A Xenon lamp having a 100 $mWcm^{-2}$ light intensity was used as an illumination source. The cells active area attained 0.19 cm^2. From I-V curves, efficiency, short circuit current density, open circuit voltage, and fill factor were computed.

3. Results and discussion

Figure 1 expresses UV-visible spectrum of CIS and CIS/ZnS but no well-defined excitonic peak have revealed. Such criteria are distinctive for Zn–Cu–In–S quaternary sets, mainly accompanied with sub-bandgap optical transitions including point defects [37,38].

Therefore, the optical bandgap energy of CuInS and CuInS/ZnS QD utilizing Tauc's plot (Figure 2) is appraised from the subsequent formula [39]:

$$\alpha = 2.303 \frac{A}{d} \quad (1)$$

in Eq.1, α denotes the energy-dependent absorption coefficient, A and d refer to the absorbance, and the specimen thickness, respectively. To apply Tauc's relation, a curve is plotted by correlating the photon's energy and $(\alpha h\upsilon)^2$, utilizing the subsequent equation [40].

$$\alpha h\nu = B(h\nu - E_g)^n \quad (2)$$

in Eq.2, B is a constant, h signifies the Planck's constant, E_g refers to the optical band gap energy, n signifies a factor linked to the electron transitions regime. The values of "n" vary according to the specific type of band gap: 1/2 refers to direct band gaps, 2 refers to indirect band gaps, 3/2 refers to direct allowed band gaps, and 3 refers to indirect forbidden band gaps. The E_g values for CIS and CIS/ZnS QDs attained 3.07 eV and 3.20 eV, respectively, as observed from Figure 2.a and Figure 2.b.

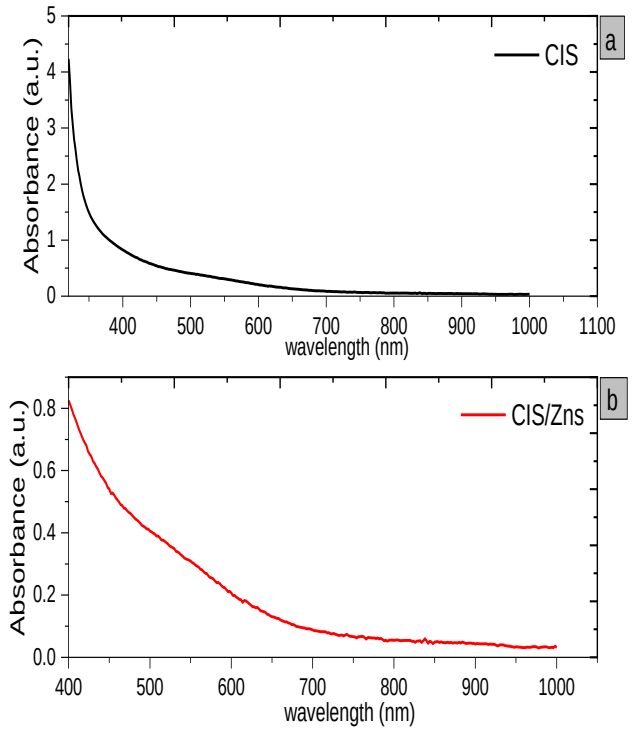

Figure 1: UV-visible spectrum for a) CIS and b) CIS/ZnS QDs

Figure 3 illustrates the CIS and CIS/ZnS QDs PL spectrum which refers to a maximum intensity at 663 nm for CIS/ZnS QDs and 750 nm for CIS QDs which indicates blue shift towards higher energy for the CIS/ZnS (core/shell) structure than CIS (core structure). This blue shift of CIS/ZnS QDs is attributed to the effect of ZnS shell which have high energy gap = 3.7 eV on the CIS core [41].

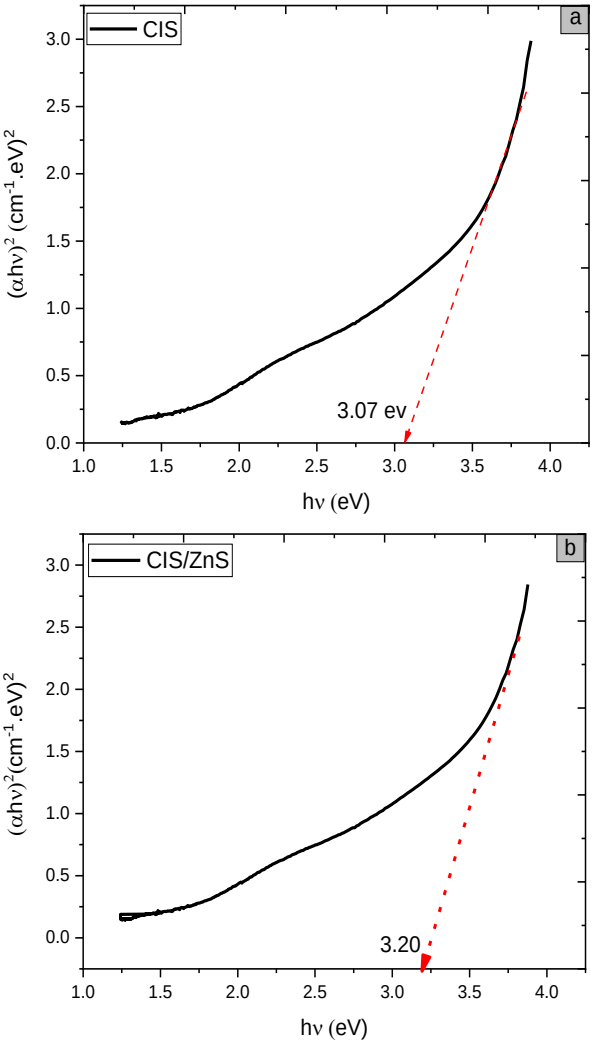

Figure 2: Tauc's plot for a) CIS and b) CIS/ZnS QDs

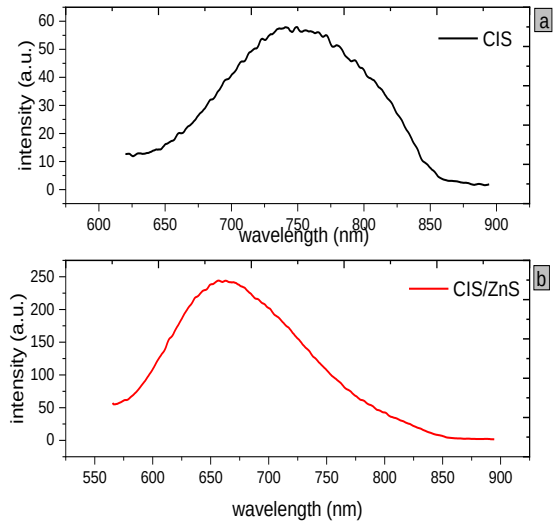

Figure 3: The PL spectrum for a) CIS and b) CIS/ZnS QDs

The X-ray diffraction (XRD) patterns of the prepared CIS and CIS/ZnS QD are shown in Figure 4-a and Figure 4-b respectively. The characteristic peaks of these QDs matched well with the XRD references (JCPDS 32-0339, CuInS2 and JCPDS 10–0434, ZnS) which confirms the tetragonal chalcopyrite structure [42–44]. The reflection peaks at 27.5°, 47.4°, and 55.3° are designated to the (111), (202), and (311) planes respectively. It was also observed that, both CIS and CIS/ZnS QDs peaks are broad which indicate their small sizes. while the peak intensities are increased with the growth of ZnS shell due to the enhancement of the crystallinity resulted from the diffusion of Zn^{2+} ions into the CIS core in the vacancies sites [45].

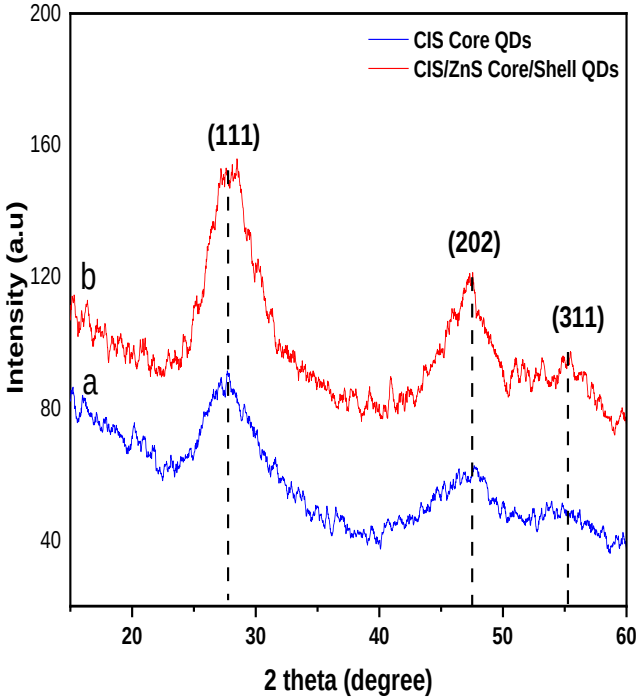

Figure 4: XRD patterns of a) CIS and b) CIS/ZnS QDs

The surface morphology of TiO_2, TiO_2/ CIS and TiO_2/ CIS/ZnS photoanodes were inspected utilizing SEM as demonstrated in Figure 5 (a, b, and c). The TiO_2 layer has relatively high pores as seen in Figure 5.a, which signifies an increased surface area and favorable environment for CIS and CIS/ZnS QDs adsorption. Figure 5.b. illustrates the adsorbed CIS QDs on TiO_2 surface with some cracks at the surface of the film. Figure 5.c. represents a homogeneous dispersion of CIS/ZnS QDs over the TiO_2 film surface. Additionally, the film exhibits a homogeneous structure without aggregations or cracks.

To examine the samples elemental composition, furthermore, the energy dispersive x-ray spectroscopy (EDX) was adopted. Figure 6 and Table 1 show EDX analysis (a) of TiO_2, (b) CIS/TiO_2 and (c) CIS/ZnS/ TiO_2 photoanodes. The analysis reveals that the prepared samples exclusively contain the elements Ti, O, S, In, Cu, Sn, and Zn. This observation suggests that the samples are pure and accurately prepared.

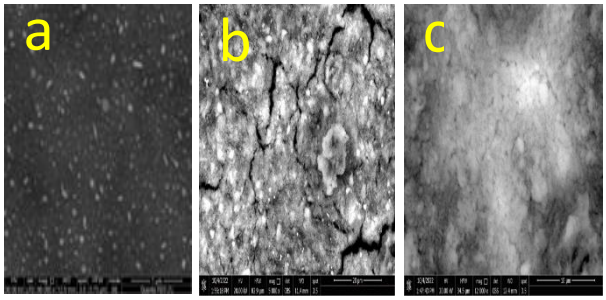

Figure 5: FESEM micrographs of: (a) TiO_2 photoanode, (b) TiO_2/CIS photoanode and (c) TiO_2/CIS/ZnS photoanode.

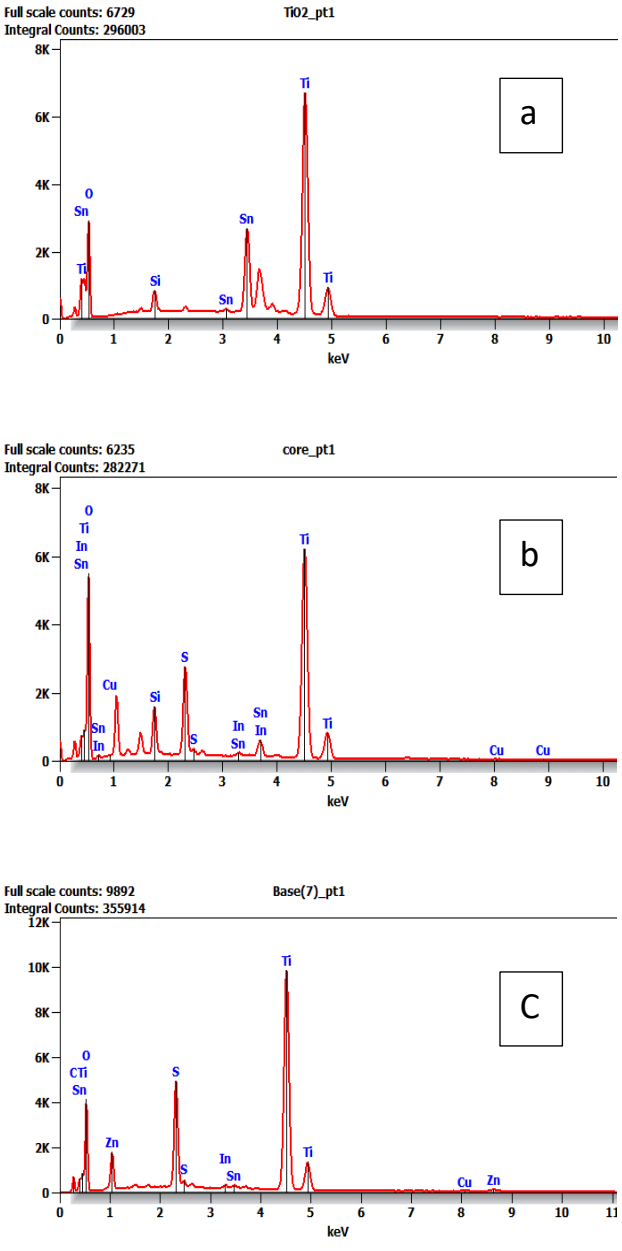

Figure 6: EDX of: (a) TiO_2, (b) CIS/ TiO_2 and (c) CIS/ZnS/ TiO_2 photoanodes respectively.

Table 1: EDX-based weight percentage for TiO_2, TiO_2 /CIS and TiO_2/CIS/ZnS photoanode.

Sample	Element (Weight percent)							
	O	Si	Ti	Sn	Cu	In	S	Zn
TiO_2	22.05	1.59	48.11	8.25	-----	-------	----	------
TiO_2/ CIS	46.21	2.80	39.88	2.36	0.26	2.27	6.22	------
TiO_2/ CIS/ ZnS	8.62	------	9.50	0.18	0.19	0.02	21.05	0.45

Figure 7 illustrates the curves of the photocurrent density voltage (J-V) of CIS/TiO_2 and CIS/ ZnS/ TiO_2 QDSSCs. Photovoltaic characteristics were evaluated within single sun (100 mw cm^{-2}) conditions and the corresponding parameters (V_{oc}, J_{sc}, FF and η) were recorded in table 2. The photoanodes have an effective area of 0.19 cm^2.

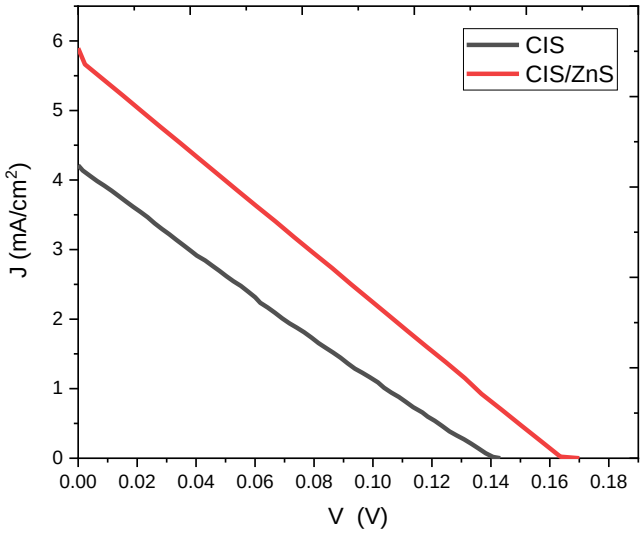

Figure 7: J-V curves for TiO_2/ CIS QDSSCs and TiO_2/ CIS/ZnS QDSSCs

It was found that, the J_{sc}, V_{oc}, and PCE also revealed an increase from 4.21 $mAcm^{-2}$, 0.14 V, and 0.13% to 5.9 $mAcm^{-2}$, 0.17 V, and 0.23% for CIS (core) and CIS/ZnS (core shell) QDSSCs, respectively. The increase in the photovoltaic parameters is attributed to core shell CuInS/ZnS QDs structure which increase energy gap from 3.07 eV to 3.20 eV as seen from Uv-vis spectroscopy and Tauc's plots. Also from SEM images, the surface homogeneity of core shell CuInS/ZnS QDs and absence of crakes provide direct bath ways and facilitate injecting excited electrons from CuInS/ZnS QDs conduction band into the TiO_2 conduction band and FTO then to counter electrode (CE). Also, the reduction of charge recombining at the interface between

electrolyte and photoanode because ZnS shell which prevent leaping of electrons into reduced electrolyte from CIS/ZnS and TiO_2 conduction band which lead to an increment in both photocurrent density and cell efficiency. On the other hand, FF showed little variation with respect to the QDs structure, as it is primarily determined by the electrolyte stability and solar cell's shunt and series resistances [46,47].

Table 2: Photovoltaic parameters for TiO_2/ CIS and TiO_2/ CIS /ZnS QDSSCs

Sample	Photovoltaic parameters			
	V_{oc} (v)	J_{sh} ($mAcm^{-2}$)	FF	η%
CIS	0.14	4.21	0.23	0.13
CIS/ZnS	0.17	5.9	0.21	0.23

Conclusions

In this study, low cost and safe QDSSCs were formulated. Cu - In - S (CIS) and Cu - In - S / ZnS (CIS/ZnS) QDs were used as a sensitizer on TiO_2 thin film. We also examined how the prepared solar cells efficiency was influenced by the core and core/shell structure. The results indicated that the utilization of the core/shell structure with CIS/ZnS QDs led to an improved photocurrent density and effectiveness. These findings indicate better contact between CIS/ZnS QDs and TiO_2 nano particles and suppressing the electron recombination in CIS/ZnS TiO_2 QDSSC. The J-V curves suggest that the TiO_2/ CIS/ZnS QDSSC exhibits the best photoelectric performance with V_{oc} = 0.17 V, J_{sc}= 5.89 $mAcm^{-2}$ and η = 0.23% which are significantly higher than those of CIS/ TiO_2 QDSSC.

References

[1] Yella A, Lee HW, Tsao HN, et al. Porphyrin-Sensitized Solar Cells with Cobalt (II/III)–Based Redox Electrolyte Exceed 12 Percent Efficiency. Science. 2011;334(6056):629-634.

[2] Kamat P V. Quantum Dot Solar Cells. Semiconductor Nanocrystals as Light Harvesters. J Phys Chem C. 2008;112(48):18737-18753.

[3] Yang Z, Chen CY, Roy P, Chang HT. Quantum dot-sensitized solar cells incorporating nanomaterials. Chem Commun. 2011;47(34):9561-9571.

[4] Santra PK, Kamat P V. Tandem-layered quantum dot solar cells: tuning the photovoltaic response with luminescent ternary cadmium chalcogenides. J Am Chem Soc. 2013;135(2):877-885.

[5] Yun HJ, Paik T, Diroll B, Edley ME, Baxter JB, Murray CB. Nanocrystal size-dependent efficiency of quantum dot sensitized solar cells in the strongly coupled CdSe nanocrystals/TiO2 system. ACS Appl Mater Interfaces. 2016;8(23):14692-14700.

[6] Cerdán-Pasarán A, Lopez-Luke T, Esparza D, et al. Photovoltaic properties of multilayered quantum dot/quantum rod-sensitized TiO 2 solar cells fabricated by SILAR and electrophoresis. Phys Chem Chem Phys. 2015;17(28):18590-18599.

[7] Kim K, Kim MJ, Kim SI, Jang JH. Towards visible light hydrogen generation: quantum dot-sensitization via efficient light harvesting of hybrid-TiO2. Sci Rep. 2013;3(1):3330.

[8] Yun J, Hwang SH, Jang J. Fabrication of Au@ Ag core/shell nanoparticles decorated TiO2 hollow structure for efficient light-harvesting in dye-sensitized solar cells. ACS Appl Mater Interfaces. 2015;7(3):2055-2063.

[9] Son S, Hwang SH, Kim C, Yun JY, Jang J. Designed synthesis of SiO2/TiO2 core/shell structure as light scattering material for highly efficient dye-sensitized solar cells. ACS Appl Mater Interfaces. 2013;5(11):4815-4820.

[10] Yu WW, Qu L, Guo W, Peng X. Experimental determination of the extinction coefficient of CdTe, CdSe, and CdS nanocrystals. Chem Mater. 2003;15(14):2854-2860.

[11] Samadpour M, Gimenez S, Zad AI, Taghavinia N, Mora-Sero I. Easily manufactured TiO 2 hollow fibers for quantum dot sensitized solar cells. Phys Chem Chem Phys. 2012;14(2):522-528.

[12] Zhu Z, Qiu J, Yan K, Yang S. Building high-efficiency CdS/CdSe-sensitized solar cells with a hierarchically branched double-layer architecture. ACS Appl Mater Interfaces. 2013;5(10):4000-4005.

[13] Alivisatos AP. Semiconductor Clusters, Nanocrystals, and Quantum Dots. Science. 1996;271(5251):933-937.

[4] de la Fuente MS, Sánchez RS, González-Pedro V, et al. Effect of organic and inorganic passivation in quantum-dot-sensitized solar cells. J Phys Chem Lett. 2013;4(9):1519-1525.

[15] Jun HK, Careem MA, Arof AK. Quantum dot-sensitized solar cells—perspective and recent developments: A review of Cd chalcogenide quantum dots as sensitizers. Renew Sustain Energy Rev. 2013;22:148-167.

[16] Cong J, Yang X, Hao Y, Kloo L, Sun L. A highly efficient colourless sulfur/iodide-based hybrid electrolyte for dye-sensitized solar cells. RSC Adv. 2012;2(9):3625.

[17] Shalom M, Dor S, Rühle S, Grinis L, Zaban A. Core/CdS Quantum Dot/Shell Mesoporous Solar Cells with Improved Stability and Efficiency Using an Amorphous TiO2 Coating. J Phys Chem C. 2009;113(9):3895-3898.

[18] Mora-Seró I, Bisquert J. Breakthroughs in the Development of Semiconductor-Sensitized Solar Cells. J Phys

Chem Lett. 2010;1(20):3046-3052.

[19[Park S, Son MK, Kim SK, Jeong MS, Prabakar K, Kim HJ. The effects of electrolyte additives on the cell performances of CdS/CdSe quantum dot sensitized solar cells. Korean J Chem Eng. 2013;30(11):2088-2092.

[20] Li L, Yang X, Gao J, et al. Highly Efficient CdS Quantum Dot-Sensitized Solar Cells Based on a Modified Polysulfide Electrolyte. J Am Chem Soc. 2011;133(22):8458-8460.

[21] Mora-Seró I, Giménez S, Moehl T, et al. Factors determining the photovoltaic performance of a CdSe quantum dot sensitized solar cell: the role of the linker molecule and of the counter electrode. Nanotechnology. 2008;19(42):424007.

[22] Chang CH, Lee YL. Chemical bath deposition of CdS quantum dots onto mesoscopic TiO2 films for application in quantum-dot-sensitized solar cells. Appl Phys Lett. 2007;91(5).

[23] Diguna LJ, Shen Q, Kobayashi J, Toyoda T. High efficiency of CdSe quantum-dot-sensitized TiO2 inverse opal solar cells. Appl Phys Lett. 2007;91(2).

[24] Tubtimtae A, Wu KL, Tung HY, Lee MW, Wang GJ. Ag2S quantum dot-sensitized solar cells. Electrochem commun. 2010;12(9):1158-1160.

[25] Feng J, Han J, Zhao X. Synthesis of CuInS2 quantum dots on TiO2 porous films by solvothermal method for absorption layer of solar cells. Prog Org Coatings. 2009;64(2-3):268-273.

[26] Plass R, Pelet S, Krueger J, Grätzel M, Bach U. Quantum Dot Sensitization of Organic−Inorganic Hybrid Solar Cells. J Phys Chem B. 2002;106(31):7578-7580.

[27] Chen F, Yao Y, Lin H, et al. Synthesis of CuInZnS quantum dots for cell labelling applications. Ceram Int. 2018;44:S34-S37.

[28] Zhang B, Wang Y, Yang C, et al. The composition effect on the optical properties of aqueous synthesized Cu–In–S and Zn–Cu–In–S quantum dot nanocrystals. Phys Chem Chem Phys. 2015;17(38):25133-25141.

[29] Adel R, Ebrahim S, Shokry A, Soliman M, Khalil M. Nanocomposite of CuInS/ZnS and nitrogen-doped graphene quantum dots for cholesterol sensing. ACS omega. 2021;6(3):2167-2176.

[30] Park JC, Nam YS. Controlling surface defects of non-stoichiometric copper-indium-sulfide quantum dots. J Colloid Interface Sci. 2015;460:173-180.

[31] Park J, Kim SW. CuInS2/ZnS core/shell quantum dots by cation exchange and their blue-shifted photoluminescence. J Mater Chem. 2011;21(11):3745.

[32] Jun HK, Careem MA, Arof AK. Efficiency improvement of CdS and CdSe quantum dot-sensitized solar cells by TiO2 surface treatment. J Renew Sustain Energy. 2014;6(2).

[33] Shen Q, Kobayashi J, Diguna LJ, Toyoda T. Effect of ZnS coating on the photovoltaic properties of CdSe quantum dot-sensitized solar cells. J Appl Phys. 2008;103(8).

[34] Samadpour M, Giménez S, Boix PP, et al. Effect of nanostructured electrode architecture and semiconductor deposition strategy on the photovoltaic performance of quantum dot sensitized solar cells. Electrochim Acta. 2012;75:39-147.

[35] Hossain MA, Jennings JR, Shen C, et al. CdSe-sensitized mesoscopic TiO2 solar cells exhibiting >5% efficiency: redundancy of CdS buffer layer. J Mater Chem. 2012;22(32):16235.

[36] Kim J, Choi H, Nahm C, et al. The role of a TiCl4 treatment on the performance of CdS quantum-dot-sensitized solar cells. J Power Sources. 2012;220:108-113.

[37] Kobosko SM, Kamat P V. Indium-rich AgInS2–ZnS quantum dots—Ag-/Zn-dependent photophysics and photovoltaics. J Phys Chem C. 2018;122(26):14336-14344.

[38] Amaral-Júnior JC, Mansur AAP, Carvalho IC, Mansur HS. Tunable luminescence of Cu-In-S/ZnS quantum dots-polysaccharide nanohybrids by environmentally friendly synthesis for potential solar energy photoconversion applications. Appl Surf Sci. 2021;542:148701.

[39] Elkony Y, Ali M, Ebrahim S, Adel R. High photoluminescence polyindole/CuInS quantum dots for Pb ions sensor. J Inorg Organomet Polym Mater. 2022;32(8):3106-3116.

[40] Barman B, Bangera K V, Shivakumar GK. ZnxSn1-xS thin films: A study on its tunable opto-electrical properties for application towards a high efficient photodetector. Sol Energy. 2020;206:479-486.

[41] Wang, Huiqing, et al. "Full-color-emitting (CuInS 2) ZnS-alloyed core/shell quantum dots with trimethoxysilyl end-capped ligands soluble in an ionic liquid." RSC advances 9.44 (2019): 25576-25582. 2018;6(20):9629-9641.

[42] Chen, Yanyan, et al. "Green and facile synthesis of water-soluble Cu–In–S/ZnS core/shell quantum dots." Inorganic chemistry 52.14 (2013): 7819-7821.

[43] Zhang, Aidi, et al. "Non-blinking (Zn) CuInS/ZnS quantum dots prepared by in situ interfacial alloying approach." Scientific reports 5.1 (2015): 15227.

[44] Lee, Jun, and Chang-Soo Han. "Large-scale synthesis of highly emissive and photostable CuInS 2/ZnS nanocrystals through hybrid flow reactor." Nanoscale research letters 9 (2014): 1-8.

[45] Ali, Magdy, et al. "Structural and optical properties of upconversion CuInS/ZnS quantum dots." Optical Materials 86 (2018): 545-549.

[46] Gayen RN, Chakrabarti T. Effect of series and shunt

resistance on the photovoltaic properties of solution-processed zinc oxide nanowire based CZTS solar cell in superstrate configuration. *Mater Sci Semicond Process*. 2019;100:1-7.

[47] Chiang YH, Lin KY, Chen YH, et al. Aqueous solution-processed off-stoichiometric Cu–In–S QDs and their application in quantum dot-sensitized solar cells. *J Mater Chem A*.